Electron transfer in the *Rhodobacter sphaeroides* reaction center assembled with zinc bacteriochlorophyll

Su Lin[a,b,1], Paul R. Jaschke[c], Haiyu Wang[a,2], Mark Paddock[d], Aaron Tufts[b], James P. Allen[b], Federico I. Rosell[e], A. Grant Mauk[e], Neal W. Woodbury[a,b], and J. Thomas Beatty[c]

[a]The Biodesign Institute at Arizona State University, Arizona State University, Tempe, AZ 85287-5201; [b]Department of Chemistry and Biochemistry, Arizona State University, Tempe, AZ 85287-1604; Departments of [c]Microbiology and Immunology and [e]Biochemistry and Molecular Biology, University of British Columbia, 2350 Health Sciences Mall, Vancouver, BC, Canada V6T 1Z3; and [d]Department of Physics, University of California at San Diego, La Jolla, CA 92093

Edited by Graham R. Fleming, University of California, Berkeley, CA, and approved April 10, 2009 (received for review December 14, 2008)

The cofactor composition and electron-transfer kinetics of the reaction center (RC) from a magnesium chelatase (*bchD*) mutant of *Rhodobacter sphaeroides* were characterized. In this RC, the special pair (P) and accessory (B) bacteriochlorophyll (BChl) -binding sites contain Zn-BChl rather than BChl *a*. Spectroscopic measurements reveal that Zn-BChl also occupies the H sites that are normally occupied by bacteriopheophytin in wild type, and at least 1 of these Zn-BChl molecules is involved in electron transfer in intact Zn-RCs with an efficiency of >95% of the wild-type RC. The absorption spectrum of this Zn-containing RC in the near-infrared region associated with P and B is shifted from 865 to 855 nm and from 802 to 794 nm respectively, compared with wild type. The bands of P and B in the visible region are centered at 600 nm, similar to those of wild type, whereas the H-cofactors have a band at 560 nm, which is a spectral signature of monomeric Zn-BChl in organic solvent. The Zn-BChl H-cofactor spectral differences compared with the P and B positions in the visible region are proposed to be due to a difference in the 5th ligand coordinating the Zn. We suggest that this coordination is a key feature of protein–cofactor interactions, which significantly contributes to the redox midpoint potential of H and the formation of the charge-separated state, and provides a unifying explanation for the properties of the primary acceptor in photosystems I (PS1) and II (PS2).

magnesium chelatase mutant | photosynthetic bacterial reaction center | photosystems I and II | protein–cofactor interaction

The purple bacterial reaction center (RC) is a pigment–protein complex that is capable of converting light energy to chemical energy with quantum yield approaching 1 (1–3). Electron transfer (ET) in this RC has been extensively studied; the structure and spectroscopic features of the complex are well known, the complex is very stable, and a large variety of mutants is available. This RC also serves as a model system for understanding protein–cofactor interactions and the role that protein plays in ET (4).

The RC from *Rhodobacter* (*Rb.*) *sphaeroides* comprises 3 protein subunits, H, M, and L. As shown in Fig. 1, the RC complex binds 9 cofactors that form 2 potential ET chains (referred to as A and B) in a C2 symmetric arrangement. The "special pair" (P) is a dimer of bacteriochlorophyll (BChl) *a* molecules and is located on the periplasmic side of the cytoplasmic membrane. Two monomeric BChls (B_A and B_B, with the subscripts denoting which chain the cofactor belongs to) are present on either side of P. These are followed by 2 bacteriopheophytin (BPhe) molecules (H_A and H_B). A nonheme iron and 2 quinones (Q_A and Q_B) are near the cytoplasmic side of the RC (5, 6). When P is excited, an electron is transferred through the A branch cofactors, and then to Q_B. In the WT RC, the times for ET from P* to H_A to Q_A to Q_B are 3 ps, 200 ps, and 200 μs, respectively. The transfer from P* to H_A is thought to be via B_A.

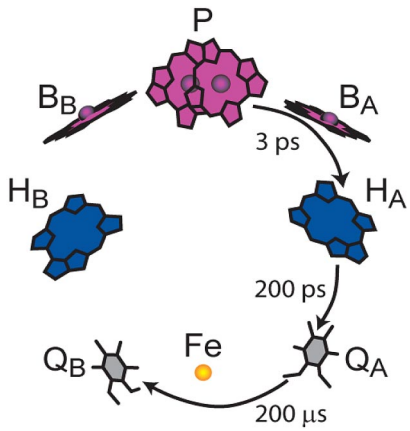

Fig. 1. Arrangement of the *Rb. sphaeroides* RC cofactors, representation of ET pathways (arrows) and the corresponding time constants. The circles in the middle of chlorins indicate the Mg atom in BChl.

The ET reactions P* to H_A to Q_A have also been studied in other species of purple bacterial RCs with varying cofactor composition, including a RC containing Zn-BChl in the P and B positions (from *Acidiphilium* (*Ac.*) *rubrum*) (7, 8) and a RC containing BChl *b* instead of BChl *a* (from *Rhodopseudomonas viridis*) (9). In all of these RCs the P and B sites contain BChl molecules, and the cofactors at the H positions are BPhe molecules. Despite shifts in the pigment absorption spectra in these species, the primary ET from P* to H_A to Q_A is essentially the same as in the *Rb. sphaeroides* RC. However, when the BPhe in the H_A-binding site of *Rb. sphaeroides* is replaced with a BChl molecule, the so-called β-mutant RC (10), the rate of ET from P* to H_A is decreased by a factor of 2. That study, together with studies of other mutants in which cofactors have been changed, indicated the importance of the energetics of the cofactors in influencing ET rates (11–14).

Recently, it was discovered that a magnesium chelatase (*bchD*) mutant of *Rb. sphaeroides* produces an RC that contains only Zn-BChl: no Mg-BChl or BPhe (we call this RC the

Author contributions: S.L. and J.T.B. designed research; S.L., P.R.J., H.W., M.P., A.T., F.I.R., and A.G.M. performed research; S.L., P.R.J., H.W., M.P., and A.T. analyzed data; and S.L., J.P.A., N.W.W., and J.T.B. wrote the paper.

The authors declare no conflict of interest.

This article is a PNAS Direct Submission.

[1]To whom correspondence should be addressed at: Department of Chemistry and Biochemistry, Arizona State University, Tempe, AZ 85287-1604. E-mail: slin@asu.edu.

[2]Present address: State Key Laboratory on Integrated Optoelectronics, College of Electronic Science and Engineering, Jilin University, 2699 Qianjin Street, Changchun 130012, China.

This article contains supporting information online at www.pnas.org/cgi/content/full/0812719106/DCSupplemental.

Zn-RC). The lack of BPhe was demonstrated both by pigment analysis and room-temperature absorption spectroscopy. In the initial study of the Zn-RC, it was proposed that the H cofactor sites are unoccupied (15).

In the work described below, detailed measurements have been used to investigate whether the H-sites in the Zn-RC are occupied, as well as to explore the mechanism of ET in this system. It is shown that the Zn-RC H cofactor sites are occupied, but by Zn-BChl instead of BPhe. Surprisingly, given the major differences in cofactor composition, the Zn-RC undergoes ET reactions with rates very similar to those of the WT *Rb. sphaeroides* RC. In contrast to all other purple bacterial RCs, in the Zn-RC the energetic differences that dictate the kinetics of ET are determined predominantly by the protein environment of 6 identical chlorin cofactors, analogous to photosystem 1 (PS1) of plants and cyanobacteria.

Results and Discussion

The RC from the *bchD* mutant of *Rb. sphaeroides* has unique spectroscopic properties because of the incorporation of Zn into BChl in place of Mg (15). In this work, spectroscopic and ET properties were investigated to address several outstanding questions. What is the cofactor composition and what are the spectroscopic signatures of the cofactors? What is the effect of Zn substitution on the redox properties of the cofactors? Does Zn substitution affect ET? What do the properties of the Zn-RC reveal about the influence of cofactor–protein interactions on ET rates?

Cofactor Composition of the Zn-RC. To evaluate the cofactor composition of the Zn-RC, steady-state absorption spectra were recorded and compared with those from the WT and β-mutant RCs. The absorption spectrum of the Zn-RC recorded at room temperature (Fig. 2*A*) shows absorption bands in the near IR region at 855 nm (due to P) and 794 nm due to the Q_Y transition of B. These spectral features are similar to those observed for WT RC containing Mg-BChl (Fig. 2*A*), except that the Zn-RC peaks are blue-shifted by 8–10 nm. The major difference between the absorption spectrum of the WT RC and the Zn-RC is the disappearance of the H band at 760 nm (due to BPhe) in the Zn-RC. Instead, a shoulder on the short-wavelength side of the B band has appeared. In the Zn-RC Q_X transition region, 2 small bands superimposed on top of a broad absorption background are observed, showing peaks at 560 and 600 nm.

The spectroscopic characteristics of P and B cofactors in the Zn-RC can be compared with published spectra of related systems. The RC of *Ac. rubrum* contains Zn-BChl in the P and B sites, but BPhe in the H sites (16). In the Q_Y transition region, the P and B absorption bands of the RC from *Ac. rubrum* are blue-shifted by 6–10 nm relative to the *Rb. sphaeroides* WT RC, consistent with the blue shift of the P and B bands observed in the Zn-RC described above, and with the proposal that the Zn-RC from the *Rb. sphaeroides bchD* mutant contains Zn-BChl at the P and B sites (15). A blue shift of the Q_Y band relative to that of the Mg-BChl is also observed for Zn-BChl in acetone/methanol (15).

The situation in the Q_X region of the spectrum is rather different. Here, there is a large blue shift of the Q_X band of Zn-BChl compared with Mg-BChl in acetone/methanol solvent: The Q_X band in solution peaks at 600 nm in Mg-BChl and at 560 nm in Zn-BChl (15). The large shift agrees well with results from previous studies that indicated that metal substitution in BChls induces a greater spectral shift of the Q_X band than the Q_Y band (17). However, the Q_X bands of P and B in the *Ac. rubrum* RC are located near 600 nm (18), similar to the P and B Q_X absorption bands in Mg-BChl-containing RCs. By analogy to *Ac. rubrum*, it appears that the Q_X transition band near 600 nm in the Zn-RC can be attributed to both B and P, although these

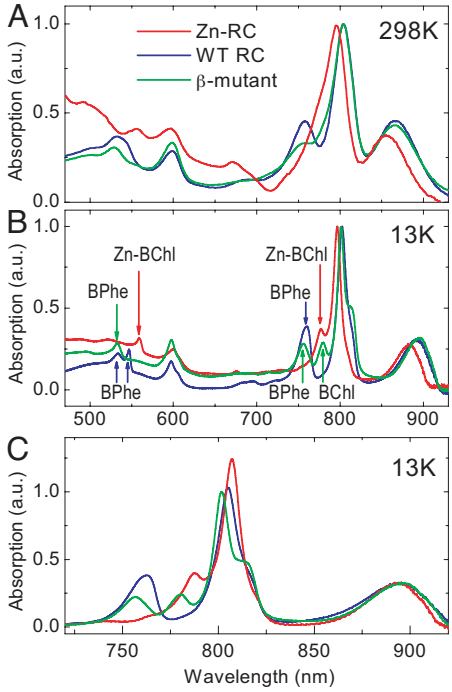

Fig. 2. Absorption spectra of RCs from the WT (blue), *bchD* mutant (red), and β-mutant (green). (*A*) At room temperature. (*B*) At 13 K. Spectra are normalized at the peak of B-band absorption near 800 nm. Arrows in *B* indicate the peaks corresponding to cofactors at H-binding sites in each sample. (*C*) Absorption spectra of the 3 RC samples in the Q_Y region normalized at the peak of P-band. The absorption spectrum of Zn-RC is mathematically red-shifted by 9 nm.

cofactors have distinct Q_Y bands at 794 and 855 nm, respectively. Why are the Q_X spectra of the P and B Zn-BChl molecules so strongly red-shifted, and what is absorbing at 560 nm and on the blue shoulder of the 794-nm band in the Zn-RC?

A study of BChls containing different metals in organic solvents concluded that tetracoordination of the central Zn in Zn-BChl results in a Q_X band in the 560-nm region, whereas a large red shift of this band (to ≈580 nm) was observed in pentacoordinated Zn-BChl (19). A study of local structures around metal atoms in Zn-BChl with and without insertion into the B sites of the *Rb. sphaeroides* strain R-26 RC, indicated that the Q_X band position of Zn-BChl at the B sites is almost identical to that of the native R-26 RC because of a fifth ligand to the Zn-BChl metal (20). A similar pentacoordination appears to exist for the P and B sites in the Zn-RC because of histidine (His) ligands (5). Thus, the Zn-BChls at the P- and B-binding sites appear to be pentacoordinated in the Zn-RC, which, along with other protein interactions, shifts the Q_X bands of P and B to ≈600 nm. Note that the Q_X band of Mg-BChl in solution (≈600 nm) is at the same position as the Q_X bands of P and B in the WT RC because the preferred coordination number of the central Mg is 5 (21).

To better understand the H site cofactor composition of the Zn-RC, the absorption spectrum was compared with that of the β-mutant RC (Fig. 2*A*). In the β-mutant RC, the amino acid leucine at M214 is replaced with a His, resulting in the replacement of the BPhe at the H_A position with a BChl molecule (10). Therefore, the β-mutant RC contains 5 BChls and 1 BPhe. Compared with the WT RC, the β-mutant RC has lower amplitude H bands at 545 (Q_X) and 760 nm (Q_Y), accompanied by a slight increase in the 600-nm band and the appearance of a shoulder on the short-wavelength side of the Q_Y band of B. The Zn-RC absorption spectrum has a further amplitude decrease of

the 760-nm band and a corresponding increase of the ≈775-nm shoulder on the B-band. Therefore, these data indicate that the Zn-RC lacks BPhe and contains a cofactor that absorbs at ≈775 nm, analogous to the H_A BChl in the β-mutant RC.

The above-mentioned absorption band features were better resolved in low-temperature absorption spectra (Fig. 2*B*). At 13 K, the shoulder at ≈775 nm becomes a peak in the absorption spectra of both the β-mutant and the Zn-RC. The amplitude of this band is approximately 2 times greater and slightly blue-shifted in the Zn-RC spectrum compared with the β-mutant RC spectrum. Fig. 2*C* compares the Q_Y transition bands from the 13 K spectra of all 3 RCs normalized to the absorption maxima of their P bands in the 850- to 865-nm region, and with the spectrum of the Zn-RC mathematically shifted 9 nm to the red to make the P-band peaks coincident. A stepwise amplitude decrease of the 760-nm band and a corresponding increase of the ≈775-nm band is shown clearly when comparing RCs containing 2 BPhe (WT), 1 BPhe (β-mutant), and no BPhe (Zn-RC). Therefore, these data confirm that the Zn-RC lacks BPhe as determined previously (15), but indicate that the Zn-RC contains Zn-BChls that absorb at 775 nm in both of the H sites.

In the Q_X transition region of the 13 K spectrum (Fig. 2*B*), the WT RC shows bands at 533 and 546 nm, corresponding to the absorption of BPhe in the H_B and H_A positions, respectively. The Q_X transition bands of B_A, B_B, and P in the WT RC are centered around 600 nm. The β-mutant RC has only 1 BPhe band (H_B, at 533 nm) because the H_A BPhe has been replaced by BChl, resulting in an increased intensity of the 600-nm band. In the Zn-RC, only 2 Q_X bands are observed, at 560 and 600 nm. Because there are no BPhe or Mg-BChl cofactors in the Zn-RC (15), it follows that the 560-nm band must be due to a Zn-BChl. As argued above, the P and B-site Zn-BChl cofactors absorb near 600 nm. The 560-nm band, therefore, must be the Q_X band of the H-site Zn-BChls, corresponding to the 775-nm peak of the Q_Y spectrum described above. It appears that Zn-BChl in the H-site is tetracoordinated because the 560-nm peak position is similar to the Q_X band of tetracoordinated Zn-BChl in solution. The 775-nm band of this H-site Zn-BChl is somewhat red-shifted relative to the Zn-BChl Q_Y band in solution (normally 762 nm), presumably because of protein–pigment interactions (19).

Based on the above analysis, we propose that the Zn-RC from the *bchD* mutant contains 6 Zn-BChl molecules. Two of these make up P, 2 occupy the B positions, and 2 occupy the H positions. The Zn-BChls are likely in very similar environments as the BChls and BPhes in the WT RC, because the RC has proven to be structurally robust to alterations, including substitution of BPhe for BChl in the heterodimer mutant (22). Furthermore, the spectral differences observed in the Q_X region are due to differences in the metal coordination state in the Zn-BChl molecules occupying P and B positions compared with those occupying the H positions. Because there is no protein ligand in the H_A and H_B sites for a fifth coordination to the metal in these Zn-BChl molecules (5), their Q_X band remains at a wavelength similar to that observed for tetracoordinated Zn-BChl in organic solvent (19). There are 2 BPhe Q_x bands in the WT RC, thought to arise from differences in hydrogen bonding (23), and so the similarity of the Q_x transitions for Zn-BChls in the H sites indicates that the hydrogen bonding is more similar than in the WT RC.

Electrochemical and Photochemical Properties of Zn-RC Cofactors. The P_{Zn}/P^+_{Zn} midpoint potential of the Zn-RC was determined to be 515 ± 5 mV (Fig. 3), only slightly higher than the 505 ± 5 mV P/P^+ midpoint potential in the WT RC (24). The difference between the P_{Zn}/P^+_{Zn} midpoint potential of the Zn-RC and that of the WT RC is in general agreement with the relative potentials obtained for isolated Zn-BChl and Mg-BChl in organic solvents (25), and the P_{Zn}/P^+_{Zn} redox potential of RCs in membranes of *Ac. rubrum* was found to be comparable with that of *Rb. sphaeroides* (8), in agreement with our result. These findings are all consistent with the observation that only a minor increase in the midpoint potential is observed when Zn-BChls serve as the primary donor (P) in place of Mg-BChls.

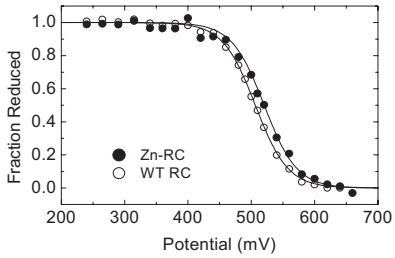

Fig. 3. Electrochemical titration of WT and Zn-RCs. The lines are fits to the Nernst equation with *n* equal to 1. The midpoint for the WT RC (open circles) is 505 ± 5 mV and for the Zn-RC (filled circles) is 515 ± 5 mV. These values were obtained by averaging the midpoint potentials of 5 independent measurements of the Zn-RC and 3 of the WT RC. For each titration, measurements were performed in both the oxidative and reductive directions to ensure reversibility.

The light-minus-dark difference absorbance spectrum was measured to examine the photoactivity of the Zn-RC (see Fig. 5*A*). The spectrum shows the bleaching of the P bands at 600 and 855 nm upon formation of the state P^+, as well as a signal with a positive band at 790 nm and a negative band at 805 nm that results from a shift of the B band due to the oxidation of P. These features are very similar to those observed with the Mg-BChl-containing WT RC. This observation further confirms the assignment of the 600- and 855-nm peaks to P in the Zn-RC steady-state absorption spectrum and suggests that ET proceeds to Q_A, producing a long-lived P^+Q^- state as is observed in the WT RC (if the ET to Q_A were not possible, the charge-separated state would decay too rapidly to be observed in a steady-state light-minus-dark difference spectrum).

Primary ET Kinetics in the Zn-RC. To characterize the primary ET processes after the photoexcitation of P, ultrafast time-resolved absorbance spectroscopy was performed on the Zn-RC at room temperature. The excited state kinetics of P (P*) monitored at 930 nm are compared with those obtained with the WT RC (Fig. 4*A*). Multiple exponential fitting of the P* kinetics of the WT RC returned 2 components of 2.8 ± 0.2 ps (86%) and 10.1 ± 0.5 ps (18%) along with a minor nondecaying component (≈4%) as seen previously (26). The Zn-RC kinetics of P* decay at 930 nm are surprisingly similar to that observed in the WT RC, showing 2 dominant decay components of 2.6 ± 0.2 ps (78%) and 9.8 ± 0.5 ps (26%) and a nondecaying component of 4%. The WT RC kinetics of 840-nm absorption changes (P ground state bleaching) show no recovery of the P band over a 3-ns time scale (Fig. 4*B*) because the $P^+Q^-_A$ state lives for milliseconds. There was also little recovery of the P bleaching at 840 nm in the Zn-RC on the 3-ns timescale, although a small amplitude decay with a time constant of 130 ps and an amplitude ≈5% of the total bleaching signal was observed (Fig. 4*B*). The slow recovery of the P ground-state bleaching in the Zn-RC, in contrast to the dominant 2.6-ps P* decay kinetics, suggests a very high yield of P^+ formation (again similar to the WT RC) with the charge-separated state being stable for at least several nanoseconds. The small amount of decay of P^+ on the hundred-picosecond time scale probably reflects a yield loss, likely due to the recombination of $P^+B^-_A$, and there seems to be a small portion of P^+ decaying on the tens of nanoseconds time scale, perhaps due to the loss of Q_A in some Zn-RCs.

To obtain additional information about the Zn-RC H_A states, time-resolved absorption spectra in the Q_X transition region

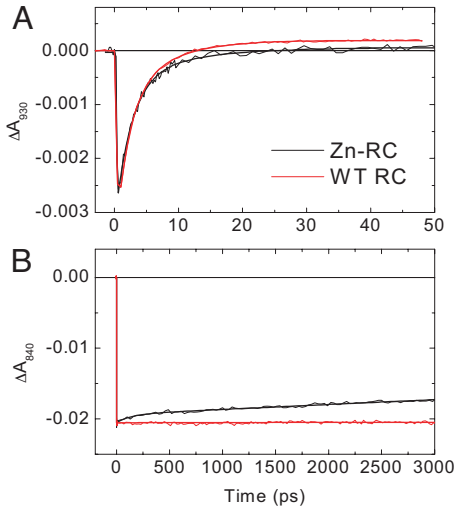

Fig. 4. Kinetics of P after femtosecond laser excitation at 860 nm in WT RC (red curves) and Zn-RC (black curves) measured at 930 nm (P*) (*A*) and 840 nm (P ground state bleaching) (*B*). The smooth curves were obtained from multiple exponential fittings to the data. The kinetic traces from the Zn-RC and the WT RC were normalized at the maximum bleachings. The fitting parameters are listed in Table 1.

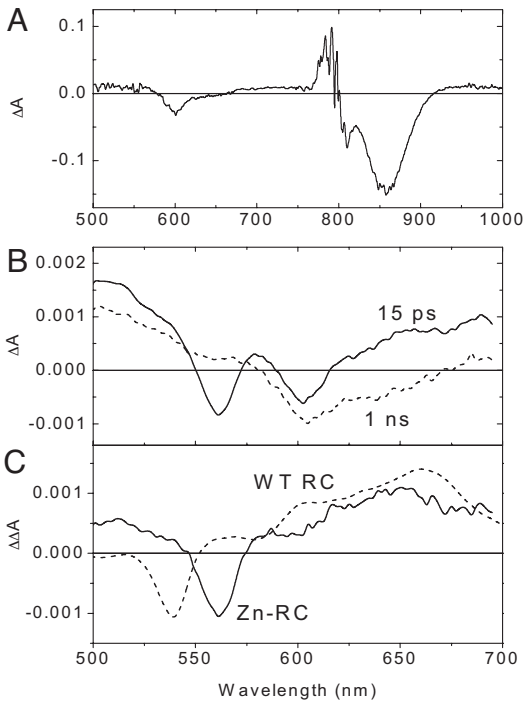

Fig. 5. Absorption difference spectrum of the Zn-RC. (*A*) Light-minus-dark spectrum of the Zn-RC, representing the P^+ state. (*B*) Time-resolved absorbance changes in the Q_X region recorded at 15 ps (solid line, $P^+H_A^-$), and 1 ns (dashed line, $P^+Q_A^-$) after laser excitation. (*C*) The difference spectrum calculated by subtracting the Zn-RC 1-ns spectrum from the 15-ps spectrum (solid line); the dashed line is a calculated difference spectrum (15 ps − 1 ns) of WT RC.

were recorded at 15 ps and 1 ns after laser excitation (Fig. 5*B*). The 15-ps spectrum represents the $P^+H_A^-$ state with the characteristic bleachings at 560 nm (H) and 600 nm (P), as well as an absorption increase >620 nm due to H_A^-. The spectrum at 1 ns shows the recovery of the H band (at 560 nm), whereas the P band bleaching persists, which is consistent with a $P^+Q_A^-$ spectrum. The difference spectrum, calculated by subtracting the 1-ns spectrum from the 15-ps spectrum, therefore, represents the H_A^- minus H_A spectrum (Fig. 5*C*). This spectrum obtained from the Zn-RC is similar to that obtained from the WT RC (26) but with the major absorbance decrease at 560 nm red-shifted by ≈20 nm from the WT value, consistent with a change in the H_A cofactor from BPhe to Zn-BChl.

To further investigate ET processes involving H_A, kinetics at 560 nm and 660 nm in the Zn-RC were measured (Fig. 6 *A* and *B*). The kinetic trace at 560 nm represents the appearance and decay of the ground-state bleaching of Zn-BChl in the H site (H_A), whereas the kinetics at 660 nm reflect the formation and decay of H_A^-. The traces at both wavelengths can be adequately fitted by a 3-ps component corresponding to the formation of $P^+H_A^-$; a 250 ± 25-ps recovery, likely due to the ET from H_A^- to Q_A; and a nondecaying component on the time scale measured, due to the contribution of long-lived P^+. The Zn-RC time constants are, again, very similar to those observed from the WT RC (26).

The fact that the kinetics of ET are essentially unaffected by simultaneously replacing Mg with Zn in all BChl cofactors and replacing BPhe with Zn-BChl is more difficult to explain than the changes in the ground-state absorption spectrum. Previous studies showed that the replacement of cofactors at either the H or B positions has a great impact on ET kinetics and can even alter the ET pathway (10, 27, 28). In the β-mutant RC, BPhe at the H_A position is replaced with a BChl, and the primary ET rate from P to H_A changes from 3.5 ps in the WT RC to 6.5 ps (10). In the so-called ϕ-mutant, the BChl at the B_B position is replaced with a

Table 1. Multiple exponential fitting parameters for kinetic curves shown in Fig. 4

Kinetics	τ_1, A_1%	τ_2, A_2%	τ_3, A_3%
WT RC (930 nm)	2.8 ps, 86%	10.1 ps, 17.7%	ND, −3.7%
Zn-RC (930 nm)	2.6 ps, 78%	9.8 ps, 26.2%	ND, −4.2%
WT RC (840 nm)			ND, 100%
Zn-RC (840 nm)		130 ps, 5.5%	ND, 94.5%

ND, non-decaying component that has a lifetime >100 times longer than the time scales measured.

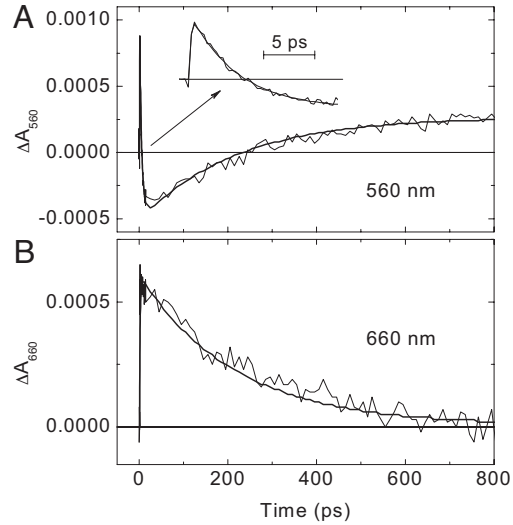

Fig. 6. Kinetics of absorption changes after laser excitation of the Zn-RC at 560 nm (*A*) and at 660 nm (*B*). The smooth curves were obtained from multiple exponential fitting to the data. The *Inset* in *A* gives the absorption changes over the first 15 ps, plotted on an expanded time scale.

BPhe, causing 35% of ET through the B-side cofactors (27). One would think that the cofactor changes in the Zn-RC would have an impact comparable with those in the mutants described above. However, the ET steps from P to Q_A in the Zn-RC take place with rates and yields very similar to the WT RC.

The insensitivity of the primary ET rates to the difference in cofactor composition between the Zn-RC and WT RC is remarkable, particularly considering the inherent energetic differences between BChl and BPhe molecules (17). However, as explained below, the observed similarity between the Zn-RC and WT RC in the kinetics for the formation of the $P^+H_A^-$ state could be because the measured time constant for the P* to H_A ET is more sensitive to the microscopic rate constant of the P* to $P^+B_A^-$ reaction than of the $P^+B_A^-$ to $P^+H_A^-$ reaction. If the 2-step model for ET holds, then ET from P* to B takes 3 ps, whereas the transfer from B_A^- to H_A takes <1 ps, and so the first ET step is rate-limiting. One would expect that the P* to $P^+B_A^-$ step would be similar in the Zn-RC and the *Ac. rubrum* RC because the 2 share the identical cofactors in the P and B sites. Because the *Ac. rubrum* and *Rb. sphaeroides* WT RCs have the same kinetics, it would not be surprising for the Zn-RC and the WT RC to have the same kinetics for the initial ET. Therefore, a moderate change in the kinetics of $P^+B_A^-$ to $P^+H_A^-$ would not affect the observed P* kinetics significantly. In other words, the energy of $P^+H_A^-$ can be varied to a certain extent without causing a major change in the P*-to-H_A ET rate. This agrees with studies of RC mutants indicating that the initial ET rate is more sensitive to the energy changes in B and less sensitive to changes in H (29).

Furthermore, although the cofactors in the Zn-RC are different from those of the WT RC, the oxidation potential of P and the reduction potential of H_A may change in a coordinated fashion (due to the influence of the protein) such that the energy difference between P* and $P^+H_A^-$ (and therefore the driving force) remain essentially the same. The blue-shifted absorption band, and the corresponding fluorescence emission band, of P in the Zn-RC suggests a higher P* energy than that of P* in the WT RC. The P_{Zn}/P_{Zn}^+ midpoint potential for the Zn-RC was determined to be 10 mV higher than that of the WT RC. What is unclear is the magnitude of the change in redox potential when BPhe is replaced with Zn-BChl at the H positions. The redox potential of H_A in RCs cannot be measured directly from isolated RCs in buffer because such negative potentials degrade the RC. However, in the Zn-RC, the metal of Zn-BChl in the H sites is very likely tetracoordinated, as argued above. Previous studies of metal-substituted BChl showed a significant difference in redox potential between BPhe and Zn-BChl in organic solvents (19) and indicated that the redox potential is linearly correlated with the Q_X transition band position. The fact that the Q_X band of the Zn-RC H positions peaks at 560 nm, closer to that of the BPhe band at 545 nm (in the WT RC) than to that of the P or B bands at 600 nm, indicates that the electronic configuration and thus the redox potential of the Zn-BChl at the H_A site is more similar to BPhe than to that of the P or B BChls. Therefore, a prediction based on Q_X band absorption wavelength would indicate a similar driving force for ET from P* to H_A in the Zn- and WT RCs of *Rb. sphaeroides* and similar ET rates.

The observed H_A^- to Q_A ET rate is also similar between Zn- and WT RCs. This makes sense if the Zn-BChl replacing BPhe at the H position in the Zn-RC is tetracoordinated, and there is only a modest change in reduction/oxidation potential of H_A, keeping the rate of ET to Q_A approximately the same in the Zn- and WT RCs. Other studies have indicated that changing the environment of H_A only weakly influences the ET rate from H_A to Q_A (29). In the WT RC, only a minor effect on the rate change (within 10%) was seen when the driving force for H_A^- to Q_A was lowered by as much as 150 mV by the substitution of various quinones at the Q_A site (30). It appears that ET from H_A^- to Q_A is optimized to be close to the maximum of the rate vs. free energy relationship and therefore rather insensitive to slight changes in driving force.

Q_A-to-Q_B ET Rate and Yield. The rate of ET from Q_A^- to Q_B in the Zn-RC was determined from absorbance changes at 775 nm (where the Q_B^--minus-Q_A^- difference spectrum has a maximum) to be ≈400 μs. The formation of P^+ in intact Zn-RCs (i.e., those containing Q_A) monitored at 860 nm (see *SI Text* and Fig. S1) was found to be ≈95% relative to the WT RC [assuming that the WT RC has a quantum yield of unity (1–3)]. The ground-state recovery of the $P^+Q_A^-$ and $P^+Q_B^-$ state takes 100 ms and ≈1 s in the WT RC, respectively (1). In the Zn-RC, the ground-state recovery of P shows 2 decay phases of 97 ms and 0.93 s. By analogy to the WT RC, the slow phase is attributed to the recombination of $P^+Q_B^-$, and the fast phase is attributed to the recombination of $P^+Q_A^-$, due to the absence of Q_B in a fraction of the RCs (31, 32).

Insight into Different Evolutionary Strategies of PS1 and Photosystem II (PS2) RCs. Our results may enable a deeper understanding of the structure, function, and evolution of RCs in general. The cyanobacterial and plant PS2 RCs have an arrangement of chlorins similar to the purple bacterial WT RC: In both cases, P is a (B)Chl dimer, B sites contain (B)Chl, and H sites contain (B)Phe (33). In contrast, the cyanobacterial and plant RCs in PS1 have 6 Mg-containing Chls in a similar spatial arrangement, analogous to the Zn-RC, with the A_0 Chl in the PS1 RC equivalent to the H_A BPhe in the WT RC (34, 35). It is interesting to note that in the PS1 RC protein, in contrast to the His residues coordinating the center Mg of the Chl molecules of P700, the sulfur of a methionine (Met) side chain weakly ligates the Mg in the Chl electron acceptor A_0. This sulfur coordination of Mg is uniquely found in RCs that contain a Chl (as opposed to a Phe) as the primary electron acceptor A_0 (34, 36). It was shown that changing the Met residue at this site to His reduces the rate of ET from P to A_0 (37), indicating that the weak ligation of the Mg in the A_0 Chl to Met in the PS1 RC results in an interaction that resembles tetracoordination, which we suggest is a key factor in governing the midpoint potential and hence the rate of ET in RCs.

We speculate that evolution has resulted in 2 strategies for a high rate of ET in RCs: (*i*) in the PS2-type of RCs, the primary electron acceptor is a (B)Phe surrounded by protein that excludes (B)Chl and water from the H sites; (*ii*) in the PS1-type of RCs, the primary acceptor is a Chl (A_0), but Chl functions well as the primary acceptor because the Mg in the A_0 Chl is ligated weakly by a sulfur atom coming from the protein, endowing this Chl with tetracoordination-like electrochemical properties.

Materials and Methods

RC Isolation. The WT *Rb. sphaeroides* strain NCIB8253 and the *bchD* mutant TB59 were grown as described previously, by using LB medium (pH 7, containing 12.8 μM Zn^{2+}) (38). The construction and expression of the mutant M214LH and RCs isolation were described previously (10, 39).

Steady-State Absorption Spectroscopy. Absorption spectra were recorded with a spectrophotometer (Cary 6000I; Varian Inc.). Low-temperature measurements were done with a closed-cycle He cryostat (Omniplex OM-8; ARS Inc). RCs were prepared in 15 mM Tris·HCl (pH 8.0), 1 mM EDTA, and 0.025% LDAO and diluted 1:1 with glycerol. Samples were deposited between 2 quartz windows separated with a spacer. The assembly was then mounted on a sample rod and frozen rapidly to ≈10 K.

P_{Zn}/P_{Zn}^+ Redox Midpoint Potential. Measurements were made at room temperature by using a thin-layer electrochemical cell as previously described (24, 40). RC samples were concentrated to an A_{792} of ≈100 and poised at 60 mM KCl in 15 mM Tris·HCl at pH 8. Potassium ferrocyanide (0.4 mM) and potassium tetracyano mono[1,10-phenanthroline]Fe(II)·$4H_2O$ (0.074 mM) were added as mediators. A spectrophotometer (Cary 5; Varian Inc.) was used to measure

absorption spectra because the potential was systematically varied. The extent of reduction monitored at the maximum of the dimer (P) Q_Y transition was fitted to the Nernst equation ($n = 1$) (24).

Microsecond and Millisecond Kinetic Measurements. Kinetic measurements on microsecond-to-millisecond time scales were performed on a home-built spectrometer using a Nd:YAG laser (Opotek) for actinic excitation (40 mJ per pulse, 5-ns half-width) (32). Kinetic traces were recorded on a LeCroy oscilloscope and then transferred to a PC for analysis (41).

Femtosecond Transient Spectroscopy. The femtosecond transient absorption spectroscopy was performed by using a pump–probe setup (4). Laser pulses of 1 mJ at a repetition rate of 1 KHz (100 fs at 800 nm) were generated from a regenerative amplifier system (Tsunami and Spitfire; Spectra-Physics). Part of the pulse energy (≈10%) was used to generate a white light continuum for the probe beam. The remainder was used to pump an optical parametric amplifier (OPA-800, Spectra-Physics) generating excitation pulses at 860 nm. Transient absorption changes at various wavelengths were measured by using a monochromator (SP150; Action Research Corp.) and a diode detector (Model 2032; New Focus Inc.). The relative polarization of the excitation and probe beams was set to the magic angle at 54.7°. The excitation intensities were kept <500 nJ per pulse, and the excitation spot size was 0.5 mm in diameter. RC samples were loaded in a spinning wheel with an optical path length of 1.2 mm, and a final optical density of ≈0.3 at 792 nm was used. Kinetic traces were fitted with a sum of exponentials by using a local written program ASUFIT.

ACKNOWLEDGMENTS. S.L. thanks P. Fromme and L. Fiedor for intriguing discussion. M.P. thanks E. Abresch for technical assistance. This work was supported by National Science Foundation (NSF) Grant MCB0642260 at Arizona State University, Natural Sciences and Engineering Research Council grants (to J.T.B.), and National Institutes of Health Grant GM 41637 (to M.P.). The transient spectrometer was funded by NSF Grant BIR9512970. The spectrophotometer and cryostat were funded by the Canada Foundation for Innovation Grant and operated with the Michael Smith Foundation for Health Care Research Grant (A.G.M.).

1. Kirmaier C, Holten D (1987) Primary photochemistry of reaction centers from the photosynthetic purple bacteria. *Photosynth Res* 13:225–260.
2. Woodbury NW, Allen JP (1995) The pathway, kinetics and thermodynamics of electron transfer in wild type and mutant reaction centers of purple nonsulfur bacteria. *Anoxygenic Photosynthetic Bacteria*, eds Blankenship RE, Madigan MT, Bauer CE (Kluwer Academic, Dordrecht, The Netherlands), pp 527–557.
3. Parson WW (1996) Photosynthetic bacterial reaction centres. *Protein Electron Transfer*, ed Bendall SD (BIOS Scientific, Oxford), pp 125–160.
4. Wang HY, et al. (2007) Protein dynamics control the kinetics of initial electron transfer in photosynthesis. *Science* 316:747–750.
5. Allen JP, et al. (1987) Structure of the reaction center from *Rhodobacter sphaeroides* R-26: The cofactors. *Proc Natl Acad Sci USA* 84:5730–5734.
6. Feher G, Allen JP, Okamura MY, Rees DC (1989) Structure and function of bacterial photosynthetic reaction centres. *Nature* 339:111–116.
7. Wang S, et al. (1994) Comparative study of reaction centers from purple photosynthetic bateria: Isolation and optical spectroscopy. *Photosynth Res* 42:203–215.
8. Tomi T, et al. (2007) Energy and electron transfer in the photosynthetic reaction center complex of *Acidiphilium rubrum* containing Zn-bacteriochlorophyll as studied by femtosecond up-conversion spectroscopy. *Biochim Biophys Acta* 1767:22–30.
9. Dressler K, et al. (1991) Detailed studies of the subpicosecond kinetics in the primary electron-transfer of reaction centers of *Rhodopseudomonas viridis. Chem Phys Lett* 183:270–276.
10. Kirmaier C, et al. (1991) Charge separation in a reaction center incorporating bacteriochlorophyll for photoactive bacteriopheophytin. *Science* 251:922–927.
11. Kee HL, et al. (2006) Determination of the rate and yield of B-side quinone reduction in *Rhodobacter capsulatus* reaction centers. *Biochemistry* 45:7314–7322.
12. Chuang JI, Boxer SG, Holten D, Kirmaier C (2008) Temperature dependence of electron transfer to the M-side bacteriopheophytin in *Rhodobacter capsulatus* reaction Centers. *J Phys Chem B* 112:5487–5499.
13. van Brederode ME, et al. (1999) Primary charge separation routes in the BChl : BPhe heterodimer reaction centers of *Rhodobacter sphaeroides. Biochemistry* 38:7545–7555.
14. Ridge JP, et al. (2000) An examination of how structural changes can affect the rate of electron transfer in a mutated bacterial photoreaction centre. *Biochem J* 351:567–578.
15. Jaschke PR, Beatty JT (2007) The photosystem of *Rhodobacter sphaeroides* assembles with zinc bacteriochlorophyll in a *bchD* (Magnesium chelatase) mutant. *Biochemistry* 46:12491–12500.
16. Wakao N, et al. (1996) Discovery of natural photosynthesis using Zn-containing bacteriochlorophyll in an aerobic bacterium *Acidiphilium rubrum. Plant Cell Physiol* 37:889–893.
17. Noy D, et al. (1998) Metal-substituted bacteriochlorophylls. 2. Changes in redox potentials and electronic transition energies are dominated by intramolecular electrostatic interactions. *J Am Chem Soc* 120:3684–3693.
18. Hiraishi A, Shimada K (2001) Aerobic anoxygenic photosynthetic bacteria with zinc-bacteriochlorophyll. *J Gen Appl Microbiol* 47:161–180.
19. Hartwich G, et al. (1998) Metal-substituted bacteriochlorophylls. 1. Preparation and influence of metal and coordination on spectra. *J Am Chem Soc* 120:3675–3683.
20. Chen LX, et al. (1995) An X-ray-absorption study of chemically-modified bacterial photosynthetic reaction centers. *Chem Phys Lett* 234:437–444.
21. Fiedor L (2006) Hexacoordination of bacteriochlorophyll in photosynthetic antenna LH1. *Biochemistry* 45:1910–1918.
22. Camara-Artigas A, Magee C, Goetsch A, Allen JP (2002) The structure of the heterodimer reaction center from *Rhodobacter sphaeroides* at 2.55 angstrom resolution. *Photosynth Res* 74:87–93.
23. Bylina EJ, et al. (1988) Influence of an amino-acid residue on the optical-properties and electron-transfer dynamics of a photosynthetic reaction center complex. *Nature* 336:182–184.
24. Lin X, et al. (1994) Specific alteration of the oxidation potential of the electron-donor in reaction centers from *Rhodobacter Sphaeroides. Proc Natl Acad Sci USA* 91:10265–10269.
25. Scheer H, Hartwich G (1995) Bacterial reaction centers with modified tetrapyrrole chromatophores. *Anoxygenic Photosynthetic Bacteria*, eds Blankenship RE, Madigan MT, Bauer CE (Kluwer Academic, Dordrecht, The Netherlands), pp 649–663.
26. Lin S, Taguchi AKW, Woodbury NW (1996) Excitation wavelength dependence of energy transfer and charge separation in reaction centers from *Rhodobacter sphaeroides*: Evidence for adiabatic electron transfer. *J Phys Chem* 100:17067–17078.
27. Katilius E, et al. (1999) B-side electron transfer in a *Rhodobacter sphaeroides* reaction center mutant in which the B-side monomer bacteriochlorophyll is replaced with bacteriopheophytin. *J Phys Chem B* 103:7386–7389.
28. Lin X, Williams JC, Allen JP, Mathis P (1994) Relationship between rate and free energy difference for electron transfer from cytochrome c_2 to the reaction center in *Rhodobacter sphaeroides. Biochemistry* 33:13517–13523.
29. Kirmaier C, Laporte L, Schenck CC, Holten D (1995) The nature and dynamics of the charge-separated intermediate in reaction centers in which bacteriochlorophyll replaces the photoactive bacteriopheophytin. 2. The rates and yields of charge separation and recombination. *J Phys Chem* 99:8910–8917.
30. Gunner MR, Dutton PL (1989) Temperature and $-\Delta G°$ dependence of the electron-transfer from Bph to Q_A in reaction center protein from *Rhodobacter sphaeroides* with different quinones as Q_A. *J Am Chem Soc* 111:3400–3412.
31. Vermeglio A, Clayton RK (1977) Kinetics of electron-transfer between primary and secondary-electron acceptor in reaction center from *Rhodopseudomonas sphaeroides. Biochim Biophys Acta* 461:159–165.
32. Kleinfeld D, Okamura MY, Feher G (1984) Electron-transfer in reaction centers of *Rhodopseudomonas sphaeroides.* 1. Determination of the charge recombination pathway of $D^+Q_AQ_B^-$ and free-energy and kinetic relations between $Q_A^-Q_B$ and $Q_AQ_B^-$. *Biochim Biophys Acta* 766:126–140.
33. Zouni A, et al. (2001) Crystal structure of photosystem II from *Synechococcus elongatus* at 3.8 angstrom resolution. *Nature* 409:739–743.
34. Jordan P, et al. (2001) Three-dimensional structure of cyanobacterial photosystem I at 2.5 angstrom resolution. *Nature* 411:909–917.
35. Ben-Shem A, Frolow F, Nelson N (2003) Crystal structure of plant photosystem I. *Nature* 426:630–635.
36. Fromme P, Jordan P, Krauss N (2001) Structure of photosystem I. *Biochim Biophys Acta Bioenerg* 1507:5–31.
37. Ramesh VM, et al. (2007) Replacement of the methionine axial ligand to the primary electron acceptor A_0 slows the A_0^- reoxidation dynamics in Photosystem I. *Biochim Biophys Acta Bioenerg* 1767:151–160.
38. Tehrani A, Prince RC, Beatty JT (2003) Effects of photosynthetic reaction center H protein domain mutations on photosynthetic properties and reaction center assembly in *Rhodobacter sphaeroides. Biochemistry* 42:8919–8928.
39. Goldsmith JO, Boxer SG (1996) Rapid isolation of bacterial photosynthetic reaction centers with an engineered poly-histidine tag. *Biochim Biophys Acta Bioenerg* 1276:171–175.
40. Allen JP, et al. (1996) Effects of hydrogen bonding to a bacteriochlorophyll–bacteriopheophytin dimer in reaction centers from *Rhodobacter sphaeroides. Biochemistry* 35:6612–6619.
41. Paddock ML, et al. (2005) Quinone (Q_B) reduction by B-branch electron transfer in mutant bacterial reaction centers from *Rhodobacter sphaeroides*: Quantum efficiency and X-ray structure. *Biochemistry* 44:6920–6928.